7504 *Biochemistry* **2010,** *49,* 7504–7515
DOI: 10.1021/bi100607c

BIOCHEMISTRY
including biophysical chemistry & molecular biology
Article

Intensity Borrowing via Excitonic Couplings among Soret and Q_y Transitions of Bacteriochlorophylls in the Pigment Aggregates of Chlorosomes, the Light-Harvesting Antennae of Green Sulfur Bacteria[†]

Yutaka Shibata,*[,‡] Shingo Tateishi,[§] Shosuke Nakabayashi,[§] Shigeru Itoh,[‡] and Hitoshi Tamiaki[§]

[‡]*Division of Material Science* (*Physics*), *Graduate School of Science, Nagoya University, Nagoya 464-8602, Japan, and* [§]*Department of Bioscience and Biotechnology, Faculty of Science and Engineering, Ritsumeikan University, Kusatsu, Shiga 525-8577, Japan*

Received April 20, 2010; Revised Manuscript Received July 27, 2010

ABSTRACT: Model calculations of linear dichroism (LD) and circular dichroism (CD) spectra were conducted for the chlorosomes of green sulfur bacteria, *Chlorobium phaeobacteroides* and *Chlorobium tepidum*, on the basis of the theory of delocalized exciton. The chlorosomes of *Chl. phaeobacteroides* and *Chl. tepidum* contain bacteriochlorophylls (BChls) *e* and *c* as the major light-harvesting pigments, respectively. The excitonic couplings among the Soret and Q_y transitions were considered on the basis of the "rodlike" structural model for the pigment self-aggregates in a chlorosome. Trial simulations were conducted by assuming the B_x and B_y transition-dipole vectors to be parallel to the molecular *x*- and *y*-axes, respectively. The simulation at this stage could nicely reproduce the larger splitting of the Soret band and more significant enhancement of the Q_y band upon formation of chlorosome in the BChl *e*-containing chlorosome than in the BChl *c*-containing one. Intensity borrowing was indicated to be the key mechanism inducing the enhancement of the Q_y band in the BChl *e*-containing chlorosomes. However, the simulated LD and CD spectra in the Soret region showed qualitative disagreement from the observed ones. To resolve the deviations, the directions of the B_x and B_y transition-dipole vectors and the orientations of the molecular planes of BChls were adjusted in the next stage. The fine-tuning of these parameters resulted in a striking agreement between the observed and simulated CD and LD spectra over the whole spectral range studied. The best fit was obtained when the B_x and B_y transition-dipole vectors were assumed to be rotated 25° clockwise from the molecular *x*- and *y*-axes and the molecular planes in the pigment aggregate were tilted 5° from that assumed in the original model without alteration in the direction of the molecular *y*-axis. The calculated spectral profiles were affected little by the change in the curvatures of the rod surface, showing that the optical spectra of chlorosomes were determined essentially by the local pigment arrangement, but not by the higher-order structure, of the aggregate.

The chlorosome is the main light-harvesting complex of green sulfur and filamentous bacteria (*1*, *2*). These organisms can live under very low-light-intensity conditions and then need highly efficient light-harvesting apparatus. A single chlorosome achieves a large absorption cross section by containing more than hundreds of thousands of pigment molecules in its lipid monolayer envelope (*3*, *4*). Chlorosomes attach to the interior surface of the cytoplasmic membrane, in which the photosynthetic reaction centers are embedded. Their typical sizes are ca. 200 nm × 50 nm × 25 nm and ca. 100 nm × 30 nm × 15 nm for green sulfur and filamentous bacteria, respectively. The most unique feature of the chlorosome is the fact that proteins play no roles as structural scaffolds for the pigment (*1*, *2*, *5*−*7*); the pigment molecules in a chlorosome form self-aggregates with ordered structures.

The main chlorophyllous pigment contained in a chlorosome is one of bacteriochlorophyll (BChl)[1] *c*, *d*, and *e* molecules, depending on the species. As shown in Figure 1, the substituent at the C7 position in BChl *e* is a formyl group, but it is a methyl group in BChl *c* and *d*. These BChls possessing a chlorin π-system have two well-known transition bands in the visible region, called Soret (B) and Q bands (*8*). The Soret band consists of two overlapping bands, which are hereafter designated B_x and B_y. A recent theoretical study has suggested that a charge-transfer band also contributes to the Soret region (*9*). The Q-band also consists of two bands, Q_x and Q_y. The former has only a minor absorbance intensity at a higher transition energy than the latter. The transition dipoles of Q_x and Q_y transitions have been believed to be nearly parallel to the vectors from the central Mg to the nitrogen atom in the B-pyrrole ring (the molecular *x*-axis defined in this paper) and that in the A-pyrrole ring (the molecular *y*-axis) by analogy to the case of chlorophyll (Chl) *a* (*9*−*13*). The definitions of the molecular *x*- and *y*-axes in this paper are somewhat different from those of Fragata et al. (*10*). A recent study involving a femtosecond visible-pump-infrared-probe

[†]The work was supported in part by Grants-in-Aid for Scientific Research (17750010, 21750017, and 22245030) and the 21st COE program for "the origin of the universe and matter" from the Japanese Ministry of Education, Science, Sports, and Culture (MEXT) and the Japan Society for the Promotion of Science (JSPS) as well as the Research Project for Private Universities through a matching fund subsidy from MEXT, 2009−2013.

*To whom correspondence should be addressed: Division of Material Science (Physics), Graduate School of Science, Nagoya University, Nagoya 464-8602, Japan. Telephone and fax: 81-52-789-2883. E-mail: yshibata@bio.phys.nagoya-u.ac.jp.

[1]Abbreviations: BChl, bacteriochlorophyll; Chl, chlorophyll; EM, electron microscope; LD, linear dichroism; CD, circular dichroism; LHC, light-harvesting chlorophyll−protein complex; fwhm, full width at half-maximum.

 Published on Web 07/27/2010

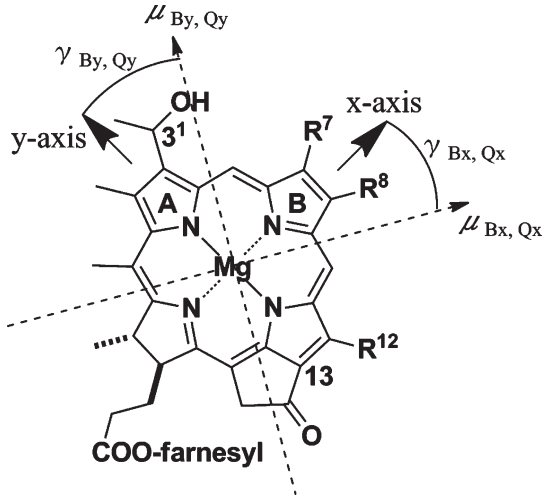

FIGURE 1: Molecular structures of representative BChl *e* (R^7 = CHO) and BChl *c* (R^7 = Me) in *Chlorobium* chlorosomes. BChls *e* and *c* in *Chlorobium* chlorosomes are mixtures of several homologues, in which R^8 = ethyl, *n*-propyl, isobutyl, or neopentyl (only in BChl *e*) and R^{12} = methyl or ethyl. The molecular *x*- and *y*-axes as defined here are shown by solid arrows. Typical directions of the transition-dipole vectors of B_x, B_y, Q_x, and Q_y bands are shown with dashed arrows.

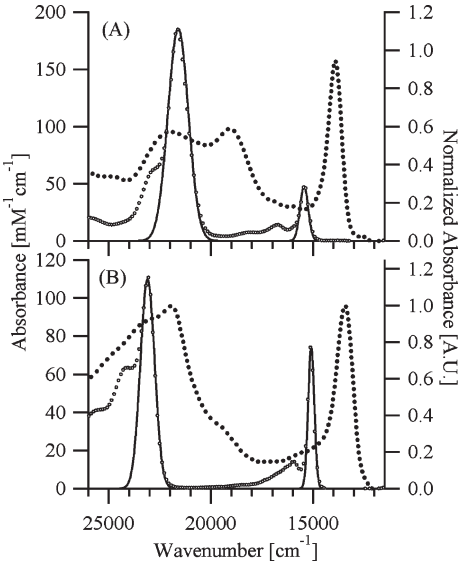

FIGURE 2: Comparison of the absorption spectra between the isolated chlorosomes (thick dotted lines) and the acetone solution of the monomeric BChls (○) that are constituents of the chlorosomes. The spectra of the monomeric BChls are shown in units of cm^{-1} mM^{-1}, while those of the isolated chlorosomes are normalized to unity at the peak wavelengths of the Q_y bands. (A) Chlorosome of *Chlorobium phaeobacteroides* and BChl *e* in acetone. (B) Chlorosome of *Chlorobium tepidum* and BChl *c* in acetone. The solid lines show the simulated curves.

experiment revealed unequivocally that the Q_y transition dipole of Chl *a* is tilted 12° from the molecular *y*-axis toward the *x*-axis (*12*, *13*). On the other hand, there has been greater uncertainty about the molecular orientation of the transition dipoles of B_x and B_y transitions.

It has been widely accepted that the adjacent molecules in the BChl aggregates of chlorosomes interact with each other through the coordination bonds between the hydroxy group at $C3^1$ and the central Mg atom as well as through the hydrogen bonds between the carbonyl group at C13 and the hydroxy group at $C3^1$. On the other hand, the higher-order supramolecular structure of the pigment aggregate in chlorosomes is still under debate. One plausible structural model has long been the rodlike model, in which the pigments are assumed to form rodlike shapes with diameters of 5−10 nm (*14*−*17*). The rodlike model was originally based on early electron microscope (EM) observations (*18*−*20*). On the other hand, the lamellar model, assuming completely different higher-order structures of aggregates, was proposed by Pšenčík et al. in 2004 on the basis of their X-ray diffraction and cryo-EM data of chlorosomes (*21*−*23*). In the lamellar model, the pigment molecules are thought to form undulate lamellar. Recent electron microscope observation at cryogenic temperatures suggested the formation of multitubular structures of variable diameters (*24*, *25*). In these studies, locally undulating lamellar-type structures were also observed. These observations seemed to suggest that the actual structure of the pigment aggregates combines the characteristics of both rodlike and lamellar models.

In densely packed pigment aggregates in a chlorosome, the excited state of the pigment molecule should be delocalized over multiple pigments. This leads to the formation of a delocalized exciton. The optical properties of an exciton reflect the structure of the pigment aggregates in chlorosomes, and those of chlorosomes have been considered as sensitive probes of the validity of the structural models of pigment aggregates. Several reports have been published on the simulation of the optical spectra considering the excitonic coupling of the Q_y band (*15*, *16*, *26*, *27*). In these studies, the absorption, circular dichroism (CD), and linear dichroism (LD) spectra of excitonic states of the pigment aggregates were calculated on the basis of the rodlike model structure. Prokhorenko et al. (*16*) demonstrated the pronounced dependence of the CD spectra on the length of the rodlike aggregate. These studies have succeeded in reproducing the experimentally obtained spectra in the Q_y band region and basically support the validity of the rodlike model. However, no report has so far been published on the theoretical calculation of the spectra of chlorosomes covering the whole spectral range involving both the Soret and Q_y band regions.

In Figure 2, we compare the absorption spectra of chlorosomes with monomeric BChl solutions in acetone. Figure 2 clearly shows significant modifications of the absorption spectra of monomeric BChls upon chlorosome formation, indicating the importance of excitonic coupling among pigments. It is conspicuous in Figure 2 that the spectral characteristic of the BChl *e*-containing chlorosomes differs considerably from that of the BChl *c*-containing chlorosomes. BChl *e* exhibits a noticeable splitting of the Soret band upon chlorosome formation, while BChl *c* does not. BChl *e* shows a significant enhancement of the Q_y absorption band upon chlorosome involvement. This is again not conspicuous in BChl *c*-containing chlorosomes. In the case of the BChl *e* monomer, the Q_y band has a much weaker intensity than the Soret band. This spectral pattern is shared with Chl *b* in plant photosynthesis, which also has a formyl group at the C7 position. Although these differences between the BChl *e*- and BChl *c*-containing chlorosomes have long been known, the mechanisms for these have not yet been thoroughly discussed.

At least, the relative enhancement of the Q_y absorption band upon chlorosome formation cannot be explained by considering only the excitonic couplings among the Q_y transitions in different molecules. The enhancement might be induced by mixing with the more intense Soret transitions. Such a mixing effect has been reported to be important in the case of the J-aggregate of

porphyrins (*28*−*30*) but not been taken into account for the chlorosomal absorption spectra. For the elucidation of the supramolecular structures of chlorosomal self-aggregates, it will be quite informative to examine whether the above phenomena can be reproduced by simulations considering excitonic couplings on the basis of certain structural models of the pigment aggregate.

In this study, we theoretically estimate the absorption, LD, and CD spectra of chlorosomes containing BChl *e* or *c*, considering, for the first time, the effects of the excitonic couplings between the Soret bands (B−B coupling) and between the Soret and Q_y bands (B−Q coupling) as well as those between the Q_y bands (Q−Q coupling). Similar studies considering the B−B, B−Q, and Q−Q couplings have been performed to reproduce the CD spectra of a light-harvesting complex of bacteria, LH1 (*31*), and of plants, LHCII (*32*). This study employs an approach similar to that of the studies mentioned above. We expect that taking into account the B−B and B−Q couplings will enable us to explain the modification in the spectra of the BChls upon chlorosome formation both in the Soret and Q_y band regions. We will show the importance of the B−B and B−Q couplings to explain the spectra of chlorosomes.

MATERIALS AND METHODS

Measurement of Linear Dichroism and Circular Dichroism Spectra. The following chlorosomes were isolated from cultured green sulfur bacteria, as reported previously (*33*): *Chlorobium phaeobacteroides* (recently renamed *Chlorobaculum limnaeum*) 1549 and *Chlorobium tepidum* (*Chlorobaculum tepidum*) WT2321 (c-strains) (*34*). LD spectra of isolated chlorosomes embedded in a polyacrylamide gel were recorded using handmade gel-compressing equipment set in a spectrophotometer (Shimadzu model UV-3100PC) according to the reported procedures (*35*, *36*). The acrylamide gel containing chlorosomes was elongated in one direction (defined as the laboratory *z*-axis) and shrunk in another direction (the laboratory *x*-axis). The width along the other direction (the laboratory *y*-axis) remained unchanged. The long axis of the chlorosomes was aligned toward the *z*-axis. The anisotropic absorption spectra were recorded by lights polarized parallel to the *x*-, *y*-, and *z*-axes.

The CD spectra were recorded with a CD spectrometer (JASCO J-720W). The sample solutions were contained in a quartz cell with an optical path length of 10 mm. The concentrations of the samples were adjusted to give an optical density of ca. 1 at the peak of the Q_y band.

Theoretical Background. The absorption spectrum, its polarization dependence, and the CD spectrum of a chlorosomal pigment self-aggregate were simulated assuming delocalized excitonic states over a large number of pigment molecules composing the aggregate. This simulation was conducted considering the B−B, B−Q, and Q−Q couplings. The transition dipoles and energy levels of the excitonic eigenstates were obtained by diagonalizing the interaction Hamiltonian matrix

$$H = \begin{pmatrix} E_{B_x} & 0 & 0 & V_{B_{x2},B_{x1}} & V_{B_{y2},B_{x1}} & V_{Q_{y2},B_{x1}} & \\ 0 & E_{B_y} & 0 & V_{B_{x2},B_{y1}} & V_{B_{y2},B_{y1}} & V_{Q_{y2},B_{y1}} & \cdots \\ 0 & 0 & E_{Q_y} & V_{B_{x2},Q_{y1}} & V_{B_{y2},Q_{y1}} & V_{Q_{y2},Q_{y1}} & \\ V_{B_{x1},B_{x2}} & V_{B_{y1},B_{x2}} & V_{Q_{y1},B_{x2}} & E_{B_x} & 0 & 0 & \\ V_{B_{x1},B_{y2}} & V_{B_{y1},B_{y2}} & V_{Q_{y1},B_{y2}} & 0 & E_{B_y} & 0 & \cdots \\ V_{B_{x1},Q_{y2}} & V_{B_{y1},Q_{y2}} & V_{Q_{y1},Q_{y2}} & 0 & 0 & E_{Q_y} & \\ & \vdots & & \vdots & & & \ddots \end{pmatrix} \quad (1)$$

Here, the diagonal elements, E_{B_x}, E_{B_y}, and E_{Q_y}, are the site energies of the B_x, B_y, and Q_y transitions, respectively. The contribution of the Q_x transition possesses only a minor intensity and was omitted in this study. The off-diagonal element with the form $V_{C_iD_j}$ is the excitonic coupling between the C-transition dipole of *i*th molecule and D-transition dipole of the *j*th molecule, where C and D are the B_x, B_y, or Q_y transition. We took into account the inhomogeneous distribution of the site energy by conducting a Monte Carlo calculation with multiple realizations of the diagonal disorders in the site energy

$$E_C = E_C^0 + \Delta E_C \quad (2)$$

where the subscript C is either B_x, B_y, or Q_y. Thus, $E_{B_x}{}^0$, $E_{B_y}{}^0$, and $E_{Q_y}{}^0$ are the averaged site energies of the B_x, B_y, and Q_y transitions, respectively, and ΔE_{B_x}, ΔE_{B_y}, and ΔE_{Q_y} are the random fluctuations inducing inhomogeneous broadening. We assumed that ΔE_{B_x}, ΔE_{B_y}, and ΔE_{Q_y} obeyed the Gaussian distributions with fwhm values of Δ_{B_x}, Δ_{B_y}, and Δ_{Q_y}, respectively.

The excitonic coupling terms in eq 1 were calculated in units of cm^{-1} on the basis of the dipole−dipole approximation

$$V_{C_i,D_j} = \frac{5.04}{n^2}\left(\frac{\boldsymbol{\mu}_{C,i}\cdot\boldsymbol{\mu}_{D,j}}{{r_{ij}}^3} - \frac{3(\mathbf{r}_{ij}\cdot\boldsymbol{\mu}_{C,i})(\mathbf{r}_{ij}\cdot\boldsymbol{\mu}_{D,j})}{{r_{ij}}^5}\right) \quad (3)$$

where $\boldsymbol{\mu}_{C,i}$ and $\boldsymbol{\mu}_{D,j}$ are the transition-dipole vectors in the debye unit of the C-transition of the *i*th molecule and that of the D-transition of the *j*th molecule, respectively. Again, C and D are the B_x, B_y, or Q_y transition. $\mathbf{r}_{ij}$ is a vector in nanometers connecting the central Mg atoms of the *i*th to *j*th molecules, and its absolute value is indicated by r_{ij}. *n* is the refractive index of the medium.

According to Knox (*37*), the absorption spectrum $\varepsilon(\nu)$ in units of M^{-1} cm^{-1} of a monomeric pigment solution can be approximately given by the following equation

$$\varepsilon(\nu) = \sum_{\substack{C= \\ B_x,B_y,Q_y}} \frac{|\boldsymbol{\mu}_C|^2}{9.19\times10^{-3}n}\frac{\nu_{shift,C}+\nu_{0,C}}{\sqrt{2\pi}\sigma_C}\exp\left\{\frac{[\nu-(\nu_{shift,C}+\nu_{0,C})]^2}{2{\sigma_C}^2}\right\} \quad (4)$$

where $\boldsymbol{\mu}_{B_x}$, $\boldsymbol{\mu}_{B_y}$, and $\boldsymbol{\mu}_{Q_y}$ are the transition-dipole vectors of the B_x, B_y, and Q_y transitions, respectively, in units of debyes. We assumed a Gaussian line shape function

$$G(\nu-\nu_{shift}-\nu_0) = \frac{1}{\sqrt{2\pi}\sigma}\exp\left\{-\frac{[\nu-(\nu_{shift}+\nu_0)]^2}{2\sigma}\right\} \quad (5)$$

where ν_0 is the 0−0 transition energy and ν_{shift} is the upshift of the peak energy of the absorption spectrum from the 0−0 transition energy due to the coupling to the phonon bath. The term $2\nu_{shift}$ can be a rough measure of the Stokes shift. ν_0, ν_{shift}, and σ in eq 4 have the subscript C, which specifies either the B_x, B_y, or Q_y transition. In the case of the monomer spectrum given by eq 4, the bandwidth σ contains the contributions from both the homogeneous and inhomogeneous broadenings. We obtain the relation between the molar extinction coefficient and the transition dipole given by Knox (*37*) by integrating both sides of eq 4 over ν with an assumption that the change in $1/\nu$ within the integral interval is negligible.

Next, we give the expression for the anisotropic absorption spectrum of pigment aggregates as a generalization of eq 4. The absorption spectrum of unidirectionally oriented pigment aggregates

measured with polarized light is given by the Gaussian-dressed stick spectrum obtained by the diagonalization of eq 1

$$A_{\mathrm{pol}}(\nu) = 3\sum_{m=1}^{3N_{\mathrm{mol}}} \frac{|\boldsymbol{\mu}_m \cdot \mathbf{e}_{\mathrm{pol}}|^2}{9.19 \times 10^{-3} n} \frac{\nu_{\mathrm{shift}} + \nu_{m0}}{\sqrt{2\pi}\sigma_m} \exp\left\{\frac{[\nu - (\nu_{\mathrm{shift}} + \nu_{m0})]^2}{2{\sigma_m}^2}\right\} \quad (6)$$

where N_{mol} is the number of pigment molecules contained in the aggregate and $\mathbf{e}_{\mathrm{pol}}$ is a unit vector parallel to the polarization of the measuring light. Because we consider the three transition bands, B_x, B_y, and Q_y, $3N_{\mathrm{mol}}$ eigenstates are involved in the calculation in eq 6. ν_{m0} and $\boldsymbol{\mu}_m$ are the 0−0 transition energy and the transition-dipole vector of the mth excitonic state, respectively. It should be noted that the standard deviation σ_m of the Gaussian line shape function in eq 6 contains only the contribution from the homogeneous broadening of the mth eigenstate. The inhomogeneous broadening was introduced as the diagonal disorders in eq 2. The factor 3 is necessary because the averaging over the random orientation distribution is not conducted in eq 6. In this study, we assumed the values of ν_{shift} to be 100 and 50 cm^{-1} for the Soret and Q_y band regions, respectively. These values are consistent with the small Stokes shift of the Q_y band of BChls or the Soret bands of porphyrins (*38*−*40*) reported so far. The transition-dipole vector, $\boldsymbol{\mu}_m$, of the mth state is related to the transition dipole of each pigment molecule as

$$\begin{aligned}\boldsymbol{\mu}_m &= \sum_{i=1}^{N_{\mathrm{mol}}} [U_{\mathrm{B}_{xi},m}\boldsymbol{\mu}_{\mathrm{B}_x,i} + U_{\mathrm{B}_{yi},m}\boldsymbol{\mu}_{\mathrm{B}_y,i} + U_{\mathrm{Q}_{yi},m}\boldsymbol{\mu}_{\mathrm{Q}_y,i}] \\ &\equiv \boldsymbol{\mu}_{\mathrm{B}_x,m} + \boldsymbol{\mu}_{\mathrm{B}_y,m} + \boldsymbol{\mu}_{\mathrm{Q}_y,m} \end{aligned} \quad (7)$$

where $U_{\mathrm{B}_{xi},m}$, $U_{\mathrm{B}_{yi},m}$, and $U_{\mathrm{Q}_{yi},m}$ are obtained from the usual eigenvalue problem of the Hamiltonian matrix eq 1 and indicates the amplitude of the B_x, B_y, or Q_y excited state of the ith molecule mixed in the mth excitoninc state. Equation 7 shows that the transition dipole of the mth state can be decomposed into the contributions from the B_x, B_y, and Q_y components, here defined as $\boldsymbol{\mu}_{\mathrm{B}_x,m}$, $\boldsymbol{\mu}_{\mathrm{B}_y,m}$, and $\boldsymbol{\mu}_{\mathrm{Q}_y,m}$, respectively. The isotropic absorption spectrum $A(\nu)$ of the pigment aggregate is expressed as

$$A(\nu) = \sum_{m=1}^{3N_{\mathrm{mol}}} \frac{|\boldsymbol{\mu}_m|^2}{9.19 \times 10^{-3} n} \frac{\nu_{\mathrm{shift}} + \nu_{m0}}{\sqrt{2\pi}\sigma_m} \exp\left\{\frac{[\nu - (\nu_{\mathrm{shift}} + \nu_{m0})]^2}{2{\sigma_m}^2}\right\} \quad (8)$$

where $A(\nu)$ is equal to $[A_x(\nu) + A_y(\nu) + A_z(\nu)]/3$, where $A_x(\nu)$, $A_y(\nu)$, and $A_z(\nu)$ are the anisotropic absorbances measured by lights polarized parallel to the x-, y-, and z-axes of the laboratory system, respectively. The CD spectrum $R(\nu)$ is given by the convolution of the rotational strengths and the same line shape function as that in eq 6

$$R(\nu) \propto \sum_{m=1}^{3N_{\mathrm{mol}}} \sum_{\substack{\mathrm{C,D} = \\ \mathrm{B}_x,\mathrm{B}_y,\mathrm{Q}_y}} \sum_{i>j} \mathbf{r}_{ij} \cdot (\boldsymbol{\mu}_{\mathrm{C},i} \times \boldsymbol{\mu}_{\mathrm{D},j}) U_{\mathrm{C}_i,m} U_{\mathrm{D}_j,m} \frac{\nu_{\mathrm{shift}} + \nu_{m0}}{\sqrt{2\pi}\sigma_m} \exp\left\{\frac{[\nu - (\nu_{\mathrm{shift}} + \nu_{m0})]^2}{2{\sigma_m}^2}\right\} \quad (9)$$

RESULTS

The goal of this study was to reproduce the optical spectra in both the Soret and Q-band regions of chlorosomes containing either BChl *e* or BChl *c* as the major pigment. Figure 3 shows the experimentally obtained CD spectra and the polarization anisotropy of the absorption spectra of chlorosomes of *Chl. phaeobacteroides* (A and B) and *Chl. tepidum* (C and D). The dashed and dotted lines in panels B and D were obtained with the chlorosome sample embedded in a compressed acrylamide gel with measuring lights polarized parallel to the gel elongation direction (the laboratory z-axis) and the gel shrink direction (the laboratory x-axis), respectively. The thick solid lines in panels B and D show the isotropic absorptions, which are the averages of the spectra obtained with measuring lights polarized parallel to the laboratory x-, y-, and z-axes. In the case of the *Chl. phaeobacteroides* chlorosome, the band at ~710 nm gained a much higher relative intensity than the Q_y band in the monomer spectrum. We hereafter designate this band as the Q_y-natured band. The absorption band in the Soret region of the chlorosome of *Chl. phaeobacteroides* split into two bands. The intensity of the band at ~530 nm exhibited a polarization dependence similar to that of the Q_y-natured band, and we designate it as the B_y-natured band. The band at ~450 nm, on the other hand, exhibited no significant dependence of the intensity on the polarization direction. We tentatively designate this band as B_x-natured.

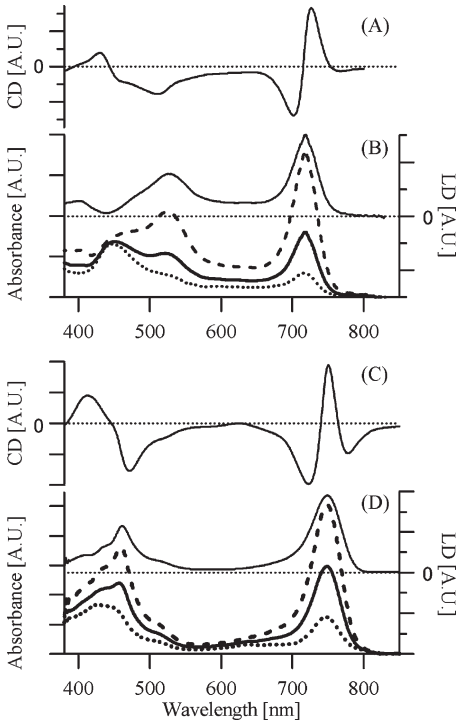

FIGURE 3: Experimentally obtained circular dichroism (A and C) and linier dichroism (B and D) spectra. The spectra in panels A and B and panels C and D are of chlorosomes purified from *Chl. phaeobacteroides* (containing BChl *e*) and *Chl. tepidum* (containing BChl *c*), respectively. The thick solid lines, dashed lines, and dotted lines show the isotropic absorption and the absorption measured by lights polarized parallel and perpendicular to the chlorosome long axis, respectively. The thin solid lines in panels A and C and panels B and D show the CD and LD spectra, respectively. The horizontal dotted lines indicate the zero lines of the CD and LD spectra.

In this study, we tried to reproduce the observed tendency shown in Figure 3 by simulating the excitonic eigenstates of the rodlike BChl aggregate. To conduct the simulation according to the formulas given in the previous section, we should determine the strengths and orientations of the transition dipoles of both the Soret and Q_y bands of monomeric BChl *e* and BChl *c*. To estimate the transition dipole strengths, we fitted the absorption

Table 1: Optical Parameters of the Monomeric BChls in Acetone Giving the Best Fit to the Observed Spectra

monomeric pigment	$\|\boldsymbol{\mu}_{B_x}\|^2$ [D^2] (E_{B_x}[cm^{-1}])	$\|\boldsymbol{\mu}_{B_y}\|^2$ [D^2] (E_{B_y}[cm^{-1}])	$\|\boldsymbol{\mu}_{Q_y}\|^2$ [D^2] (E_{Q_y}[cm^{-1}])
BChl *e*	67.2 (21500)	67.2 (21500)	19.4 (15400)
BChl *c*	26.0 (23000)	26.0 (23000)	23.0 (15050)

spectra of the monomeric BChl solutions in acetone to the simulated curves according to eq 4. We referred to the reports by Borrego et al. (*41*) and Oelze (*42*) for the values of the molar extinction coefficients of BChl *e* and BChl *c* in acetone, respectively. The solid lines in Figure 2 show the simulated absorption spectra, which successfully reproduced the main bands of the measured spectra shown by the white circles. The parameter sets giving the best fit are summarized in Table 1. As is obvious from the absorption spectra in Figure 2, the transition dipole strength is much larger for the B-band than the Q-band in BChl *e*, while the difference between the two bands is not as significant in BChl *c*.

Because the separation between the two B bands was not conspicuous in the observed monomer spectra, we assumed here the same site energy and transition dipole strength between the B_x and B_y bands. This assumption is roughly consistent with the recent results of the quantum chemical study of Chl *a* by Cai et al. (*9*). Their study suggested that the B_x and B_y bands of Chl *a* have similar oscillator strengths and transition energies and supported the early experimental results of Fragata et al. (*10*). The study by Cai et al. also pointed out that the Soret band region of Chl *a* is contributed partially from a charge-transfer band, which we omitted in our study. Any values of $|\boldsymbol{\mu}_{B_x}|$ and $|\boldsymbol{\mu}_{B_y}|$ that hold the relation $|\boldsymbol{\mu}_{B_x}|^2 + |\boldsymbol{\mu}_{B_y}|^2 = \text{constant} \equiv |\boldsymbol{\mu}_B|^2$ give the same spectral profile of the monomeric BChl in Figure 2. We here introduce a parameter $a = |\boldsymbol{\mu}_{B_x}|^2/|\boldsymbol{\mu}_{B_y}|^2$, which indicates the ratio of the contribution from the B_x transition to the Soret transition. In the following simulation, we adjust the value of *a* to reproduce the experimental spectral profiles by the simulation.

Actually, the Q_y transition-dipole vector might slightly deviate from the molecular *y*-axis, as suggested experimentally (*10*, *12*, *13*, *32*) and theoretically (*9*). The angle of the Q_y transition dipole from the molecular *y*-axis reported in the literature for Chl *a* ranges from −26° (*9*) to 7° (*32*, *43*). The wide variety in the reported values might be due to the different environment of Chl *a*. Such a slight deviation of the Q_y dipole vectors had only a minor effect on the properties of the absorption spectrum in the Q_y region of the pigment aggregate. Thus, the Q_y transition-dipole vector was assumed to be parallel to the molecular *y*-axis throughout this study. There is a much larger uncertainty about the orientations of the B_x and B_y transition-dipole vectors, which crucially affected the spectral profiles in the Soret region. In this study, we consider the orientations of the B_x and B_y transition dipoles as adjustable parameters. As shown in Figure 1, we refer to the angle between the B_y transition-dipole vector and the molecular *y*-axis and that between the B_x transition-dipole vector and the molecular *x*-axis as γ_{B_y} and γ_{B_x}, respectively. In this study, for the sake of simplicity, we assumed a right-angle crossing between the transition-dipole vectors of the B_x and B_y transitions, which led to the relation $\gamma_{B_y} = \gamma_{B_x}$.

We started the simulation on the basis of the model structure proposed by Prokhorenko et al. (*16*, *26*), which is essentially the same as that originally proposed by Holzwarth and Schaffner (*14*).

Table 2: Parameters of the Model Structures of the Rod

parameter	value
model giving the spectra in Figure 4	
φ_1	90°
θ	35.5°
φ_2	274°
Mg−Mg distance in the stack	6.75 Å
angle between the *z*-axis and the BChl plane	35.5°
surface−surface distance of BChls in a stack	3.92 Å
model giving the spectra in Figure 7	
φ_1	120°
θ	35.5°
φ_2	274°
Mg−Mg distance in the stack	6.75 Å
angle between the *z*-axis and the BChl plane	30.5°
surface−surface distance of BChls in a stack	3.39 Å

Ganapathy et al. recently proposed a more sophisticated model (*25*), in which the arrangement of the transition dipole was almost the same as that in the original one. In our study, the molecular arrangement in the rodlike model was assumed to be the same between the BChl *e*- and BChl *c*-containing chlorosomes. This assumption is considered as a working hypothesis in this study. The rod was formed from an array of molecular stacks of BChl along the rod axis. The Mg−Mg distance of the neighboring BChls in a stack was set to 6.75 Å, and the neighboring stacks were assumed to be shifted 1.68 Å along the stack. The rod radius was 26.8 Å, and the rod contained 20 stacks. A stack was assumed to contain 10 BChl molecules, resulting in it having a length of ∼6.1 nm. We here adopted single-tube aggregates. We also simulated the spectra on the basis of a double-tube aggregate model and confirmed that the qualitative tendency of the simulated spectra was not sharply influenced by the choice of a single or a double tube.

The molecular orientations of BChls in the model structure were defined as follows by using three rotation angles, φ_1, θ, and φ_2: the molecular *x*- and *y*-axes of the BChl molecule were first aligned parallel to the normal of the circumference of the rod and the rod axis, respectively. Then, the molecule was rotated φ_1 about the *z*-axis, θ about the tangent of the circumference, and φ_2 about the *z*-axis. The definition of the molecular orientation described above is schematically shown in Figure S1 of the Supporting Information. After these rotations, the angle between the molecular *y*-axis and the rod axis coincides with θ, which was assumed to be 35.5° according to Prokhorenko et al. (*16*). The parameters of the molecular orientations in the model structure are summarized in Table 2. The arrangements of the molecular *x*- and *y*-axes of BChls and their transition dipoles in our model are depicted in Figure S2 of the Supporting Information. In the first stage of the simulation, the value of φ_1 was tentatively set to 90°, which resulted in the right-angle crossing between the molecular *x*-axis and the rod axis. The deviations of the B_x and B_y transition dipoles from the molecular *x*- and *y*-axes were omitted. Thus, the molecular *x*-axes (parallel to the B_x transition-dipole vectors) shown by the red bars in Figure S2 of the Supporting Information were radially oriented around the rod. The angle between the rod axis and the molecular plane of BChl (θ) was equal to 35.5° in this case.

Figure 4 shows the simulated polarization anisotropic absorption and CD spectra of the pigment aggregates based on the structural model described above. The simulated curves are the averages over 50 realizations of the diagonal disorder sets in eq 2

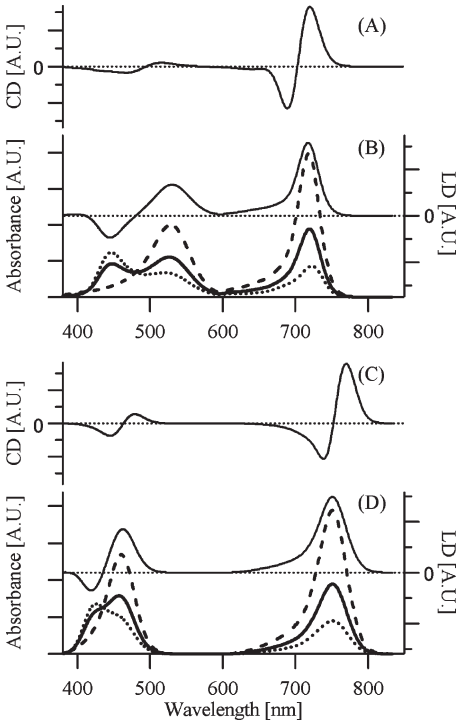

FIGURE 4: Simulated circular dichroism (A and C) and linier dichroism (B and D) spectra based on the rodlike aggregate model structure with the molecular *x*-axis parallel to the normal of the rod surface. The spectra in panels A and B and panels C and D are of the pigment aggregates in chlorosomes composed of BChl *e* and BChl *c*, respectively. The meanings of the lines are the same as those in Figure 3.

in the Monte Carlo algorithm. The dashed lines in panels B and D were calculated according to eq 6, with the polarization direction of the measuring light parallel to the *z*-axis. The dotted lines are the average of the simulated spectra with the measuring lights polarized parallel to the *x*- and *y*-axes. The thick solid lines in panels B and D are the isotropic spectra calculated according to eq 8. The value of the site energy of each band was fine-tuned by hand to fit the peak positions of the absorption bands. The fwhm of the Gaussian line shape functions was set at 1400 cm^{-1} for the Soret band and 450 cm^{-1} for the Q_y-natured band for both BChl *e*- and BChl *c*-containing chlorosomes. The former is comparable to the values used for the Soret bands of Chl *a* and Chl *b* by Georgakopoulou et al. (*32*) (fwhm of ~1330 cm^{-1}). The latter is between the values used by Prokhorenko et al. (*16*, *26*) (350 cm^{-1}) and Georgakopoulou et al. (*32*) (~500 cm^{-1}). The value of *a* was also adjusted to reproduce the observed intensity ratio between the B_x-natured and B_y-natured bands. The refractive index *n* was set at 1.4 throughout this study. This value is slightly larger than those assumed in other reports (*15*, *16*, *26*), in which refractive indexes of 1.0−1.1, much closer to the vacuum value, were used. On the other hand, Linnanto and Korrpi-Tommola (*27*) used a value of 2.1. We used the value given above because refractive indexes of <1.4 resulted in much larger Soret band splitting compared to those in the experimental results, particularly in the case of BChl *e*-containing chlorosome.

The simulation could successfully reproduce (1) a much larger splitting of the Soret band in the BChl *e*-containing chlorosome than in the BChl *c*-containing one, (2) a much more significant enhancement of the Q_y band in the BChl *e*-containing chlorosome than in the BChl *c*-containing one, and (3) the polarization dependence of the B_y-natured and Q_y-natured bands of both the BChl *e*- and BChl *c*-containing chlorosomes. The parameters giving the spectra in Figure 4 are summarized in Table 3. The large splitting of the Soret band of the BChl *e*-containing chlorosome was not due to the adjustment of the site energy values, which were modified slightly from those of the monomer. It should be noticed that the simulation predicted inversions of the transition energies of B_x and B_y as a result of the excitonic coupling. In the simulation of the BChl *e*-containing chlorosome, the transition energy of the B_y-natured band (525 nm ≅ 19050 cm^{-1}) was significantly lowered from the site energy of the B_y transition (22000 cm^{-1}), which was originally higher than that of the B_x transition (19300 cm^{-1}). This inversion also occurred in the case of the BChl *c*-containing chlorosome, although it was not noticeable. We also calculated the spectra by assuming the same site energy for B_x and B_y as a trial. These simulations, of course, could not fit the peak positions of the observed data and confirmed the much more pronounced splitting of the Soret band for the BChl *e*-containing chlorosome than for the BChl *c*-containing one. The less significant enhancement of the Q_y-natured band and the less conspicuous Soret band splitting for the BChl *c*-containing chlorosome are consistent with the experimental observations and probably due to the ~3 times weaker transition-dipole strength of the Soret band of the monomeric BChl *c*.

Although the simulated curves in Figure 4 could roughly reproduce the overall spectral profiles, we found several qualitative disagreements between the simulated and experimental spectra. The B_x-natured bands showed a negligible dependence on the polarization direction in reality, while those in the simulated curves showed sharp dependences on the polarization direction. The LD spectra, i.e., the difference between the absorption spectra observed by the light polarized parallel and perpendicular to the rod axis, were positive over the whole spectral range in the experimental spectra, while they became negative in the B_x-natured band region in the simulated one. The simulated CD spectra showed minus−plus patterns in the Soret region, while the experimental spectra showed opposite signs. Furthermore, the simulated CD spectra of the BChl *c*-containing chlorosome showed a minus−plus pattern in the Q_y region, while the experimental spectrum has a conspicuous negative band in its red edge region.

To resolve the deviations described above, we simulated the spectra allowing the parameters γ_{B_y} and γ_{B_x} to vary slightly. Figures 5A and 6A show the simulated CD and LD spectra with γ_{B_y} and γ_{B_x} equal to 0° (solid lines), −20° (dotted lines), and 20° (dashed lines) of the rodlike pigment aggregates composed of BChl *e* and BChl *c*, respectively. The other parameters were the same as those listed in Table 3. We simulated the averaged spectra over 10 realizations of the diagonal disorder sets in the Monte Carlo algorithm. The results clearly showed that slight adjustments only in the directions of the B_x and B_y transition dipoles did not improve the fitting of the LD spectra in the Soret region. Negative LD features at ~450 nm for the BChl *e*-containing chlorosome and ~420 nm for the BChl *c*-containing chlorosome could not be reduced by the adjustments. The CD spectra in the Soret region were not significantly affected either, especially in the case of the BChl *c*-containing chlorosome. Further refinement of the other parameters seemed to be required to improve the fitting.

Next, we adjusted the structural parameter of the rodlike aggregate as well as γ_{B_y} and γ_{B_x}. We fine-tuned the value of φ_1. The modification of φ_1 results in the tilt of the molecular *x*-axis from the normal of the rod surface, while the orientations of the

Table 3: Optical Parameters of the BChls Giving the Simulated Spectra of Rodlike Aggregates of BChls in Figures 4 and 7

pigment	$\|\boldsymbol{\mu}_{B_x}\|^2$ [D^2], E_{B_x}[cm^{-1}] (Δ_{B_x}[cm^{-1}])	γ_{B_x} [deg]	$\|\boldsymbol{\mu}_{B_y}\|^2$ [D^2], E_{B_y}[cm^{-1}] (Δ_{B_y}[cm^{-1}])	γ_{B_y} [deg]	$\|\boldsymbol{\mu}_{Q_y}\|^2$ [D^2], E_{Q_y}[cm^{-1}] (Δ_{Q_y}[cm^{-1}])	γ_{Q_y} [deg]
			Parameters Giving the Spectra in Figure 4			
BChl *e*	40.4, 19300 (1500)	0	94.1, 22000 (1500)	0	19.4, 15300 (600)	0
BChl *c*	16.0, 22300 (900)	0	36.0, 23000 (900)	0	23.0, 14400 (550)	0
			Parameters Giving the Spectra in Figure 7			
BChl *e*	34.5, 20000 (1450)	25	100, 22000 (1450)	25	19.4, 1530 (600)	0
BChl *c*	16.0, 22400 (850)	25	36.0, 22900 (850)	25	23.0, 14450 (550)	0

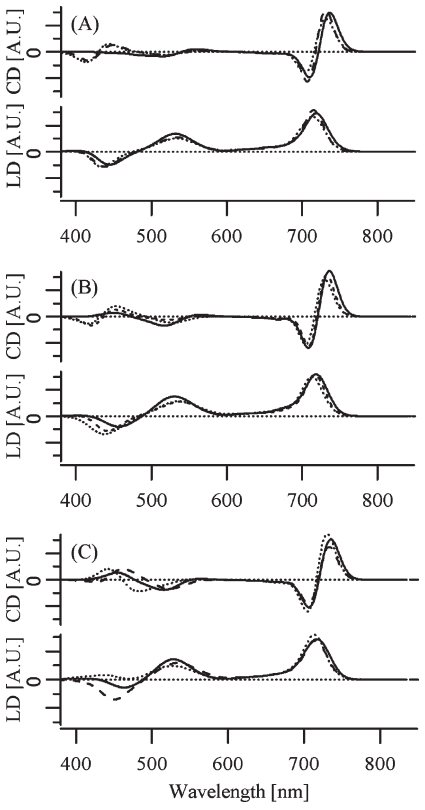

FIGURE 5: Simulated CD (top spectrum in each panel) and LD (bottom spectrum in each panel) spectra based on the rod composed of BChl *e* with various values of φ_1, γ_{B_y}, and γ_{B_x}. φ_1 = 90° (A). φ_1 = 60° (B). φ_1 = 120° (C). γ_{B_y} and γ_{B_x} = 0° (solid lines). γ_{B_y} and γ_{B_x} = 20° (dotted lines). γ_{B_y} and γ_{B_x} = −20° (dashed lines).

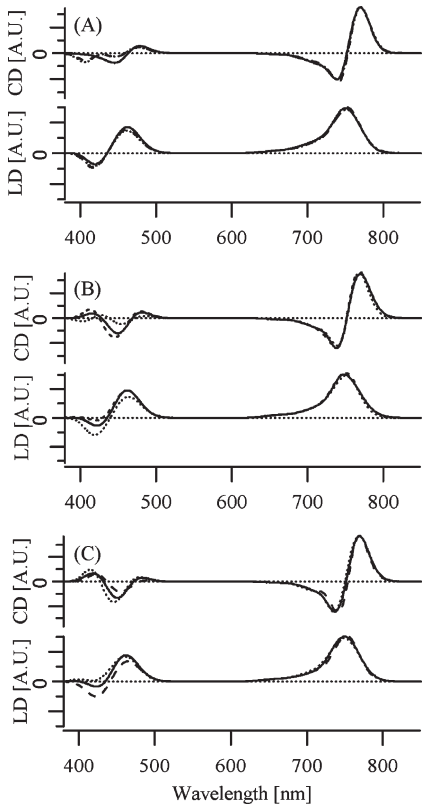

FIGURE 6: Simulated CD (top spectrum in each panel) and LD (bottom spectrum in each panel) spectra based on the rod composed of BChl *c* with various values of φ_1, γ_{B_y}, and γ_{B_x}. φ_1 = 90° (A). φ_1 = 60° (B). φ_1 = 120° (C). γ_{B_y} and γ_{B_x} = 0° (solid lines). γ_{B_y} and γ_{B_x} = 20° (dotted lines). γ_{B_y} and γ_{B_x} = −20° (dashed lines).

molecular *y*-axes remained unchanged. The modification of φ_1 from 90° reduced the angle between the *z*-axis and the molecular plane of BChls from the value of 35.5°. The OH group at C3, the CO group at C13, and the Mg atom are all located in proximity on the molecular *y*-axis. Thus, the adjustment of φ_1, which keeps the molecular *y*-axes unchanged, hardly alters the distances between the groups mentioned above. The above structural change does not seem to destroy the hydrogen bond networks and the Mg coordination bonds in the pigment aggregate. Panels B and C of Figure 5 and panels B and C of Figure 6 show the results of the simulations with a φ_1 of 60° (B) and a φ_1 of 120° (C). The curves for which γ_{B_y} and γ_{B_x} are equal to 0° (solid lines), −20° (dotted lines), and 20° (dashed lines) are shown. The fine-tuning of φ_1 together with that of γ_{B_y} and γ_{B_x} resulted in qualitative alterations in both the LD and CD spectra in the Soret region. The negative LD features around the B_x-natured band are significantly reduced when φ_1 = 60° and γ_{B_y} and γ_{B_x} = −20° (dotted lines in panel B) or when φ_1 = 120° and γ_{B_y} and γ_{B_x} = 20° (dashed lines in panel C). The parameter values listed above also resulted in plus−minus patterns in the CD spectra in the Soret region, which are similar to those in the experimental spectra. Thus, the fine-tuning of φ_1 together with γ_{B_y} and γ_{B_x} drastically improved the fitting of both the LD and CD spectra.

On the basis of the results mentioned above, we recalculated the polarization anisotropy of the absorption spectra and the CD spectra, allowing fine-tuning by hand of the values of the site energies, *a*, φ_1, γ_{B_y}, and γ_{B_x}, to achieve the best fit to the experimental spectra. Panels A and B of Figure 7 show the recalculated spectra for the BChl *e*-containing chlorosome. Slight adjustments of the site energy and *a* again allowed quantitative agreement of the peak positions of the absorption bands between the simulated and experimental observations. The simulated spectra are the averages over 50 realizations of the diagonal disorder sets. The φ_1 value of 120° and γ_{B_y} and γ_{B_x} values of 25° gave the best fit to the

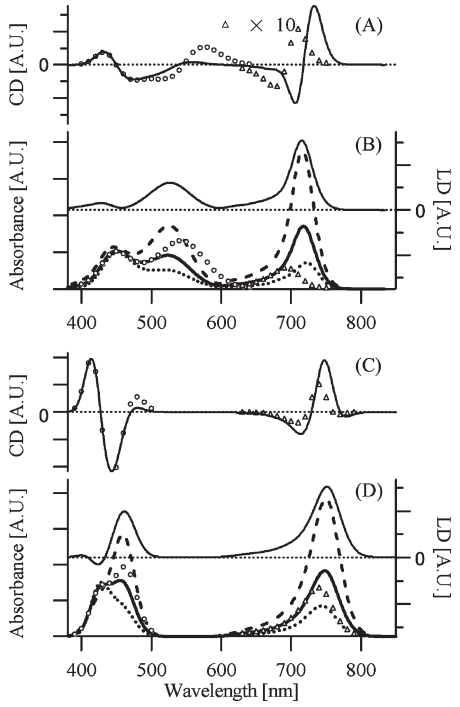

FIGURE 7: Simulated CD (A and C) and LD (B and D) spectra based on the rodlike aggregate models in which the directions of the molecular *x*-axis and the transition-dipole vectors of B_x and B_y bands were fine-tuned. The spectra in panels A and B and panels C and D are of the pigment aggregates in chlorosomes composed of BChl *e* and BChl *c*, respectively. The white circles and white triangles show the simulated spectra (CD in panels A and C and isotropic absorption in panels B and D) considering only the B−B coupling and Q−Q coupling, respectively. The simulated CD spectrum for the BChl *e*-containing chlorosome considering only the Q−Q coupling (white triangles in panel A) is magnified 10 times. The meanings of the other lines are the same as those in Figure 3.

observed profiles. The molecular arrangement of BChls in the model is shown in Figure S3 of the Supporting Information. In the case of the BChl *e*-containing chlorosome, the polarization dependences of all three bands are in excellent agreement with the experimental results shown in Figure 3. Although a small absorbance was observed in the spectral region between the Soret and Q_y bands in the experimental spectra, it is absent in the simulated ones. This discrepancy is due to the neglect of the contributions from the Q_x band, the Q_y vibronic band, and the carotenoids. The CD spectrum of the BChl *e*-containing chlorosome is also in good agreement with the experimental one.

Panels C and D of Figure 7 show the simulated spectra for the BChl *c*-containing chlorosome. The φ_1 value of 120° and γ_{B_y} and γ_{B_x} values of 25° again gave a qualitative agreement of the CD spectral pattern in the Soret region. In this case, we further modified the model structure to reproduce the minus−plus−minus pattern of the experimental CD spectrum in the Q_y region, which was characteristic for the *Chl. tepidum* chlorosome. Previous studies (*16*, *27*) have shown that the changes in the rod length affect the spectral pattern of the simulated CD spectra in the Q_y region. Thus, we assumed here a much longer rod length containing 50 molecules along the stack for the calculation of the BChl *c*-containing chlorosome. The simulated absorption and CD spectra are the average over 10 and 4 realizations of the diagonal disorder sets in the Monte Carlo procedure, respectively. The number of realizations of the diagonal disorder was reduced to 4 in the simulation of the CD spectrum, because it required too much computation time. We believe that the 4 realizations of the disorder gave satisfactorily reproducible results. Figure 7C shows that the assumption of a long rod could qualitatively reproduce the negative amplitude in the red edge region of the CD spectrum. Although the negative band is only slight, it is qualitatively similar to the observed spectra of the chlorosome of *Chl. tepidum* containing BChl *c*. The simulated absorption spectra are in good agreement with the observed ones (Figure 7D). The exception was the deviation in the carotenoid-absorbing region on the lower-energy side of the Soret band. The resultant parameters are listed in Table 3. The assumption of a long rod resulted in slightly more pronounced red shifts of the bands. Therefore, slightly higher site energies were assumed to compensate for the additional red shift.

DISCUSSION

As shown above, our analysis demonstrates that the rodlike model originally proposed by Holzwarth and Schaffner (*14*), together with slight modifications in the molecular orientations, is quite suitable for explaining the optical properties of chlorosomes not only in the Q-band region but also in the Soret region. This study indicated, for the first time, that intensity borrowing from the Soret to Q_y band significantly affects the spectral profiles of chlorosomes. To visualize the importance of the intensity borrowing, we show in Figure 7 the theoretical spectra calculated without considering B−Q coupling (white circles for the Soret region and white triangles for the Q_y region). Much less intensity was predicted for the Q_y-natured band without B−Q coupling than that with the coupling in the case of the BChl *e*-containing chlorosome, indicating the crucial importance of B−Q coupling. It was suggested that intensity borrowing was not as important in the case of the BChl *c*-containing chlorosome, in which the enhancement of the Q_y-natured band was not noticeable. Neglect of B−Q coupling also resulted in a blue shift of the Q_y-natured band for the BChl *e*-containing chlorosomes. This indicated that the mixing of the Soret transition with the Q_y-natured band contributes to its red shift.

It is noticeable that the Q_y CD band of the BChl *e*-containing chlorosome was predicted to have only a negligible amplitude in the absence of B−Q coupling. When B−Q coupling was omitted, the positive band became much more pronounced in the red edge of the Soret CD band (580 nm for the BChl *e*-containing chlorosome and 490 nm for the BChl *c*-containing one). Thus, B−Q coupling crucially affects the spectral profiles of CD. On the other hand, the LD spectra were basically the same with and without B−Q coupling except for their peak positions (data not shown). There are still several discrepancies between the simulated and experimental spectral profiles. The deviation on the higher-energy side of the Soret region might be attributable to the neglect of the charge-transfer band in this region, which was predicted in a theoretical study (*9*). Neglect of the contribution from carotenoids might also be responsible for the discrepancy.

Our conclusion seems somewhat dependent on the choice of the value of the refractive index, *n*. However, a refractive index value of 1.4 was required to obtain sufficient agreement between the experimental and simulated spectra. As described in the Results, if we set the value of *n* closer to the vacuum value as done in the previous studies (*15*, *16*, *26*), the simulation predicted a much larger splitting of the Soret band. Then, unrealistically high values were required for the site energy of the B_y to obtain a satisfactory agreement of the peak position of the B_y-natured band between the simulated and experimental spectra. On the

other hand, refractive indexes of >1.4 resulted in insufficient enhancement of the Q_y band in the case of the BChl *e*-containing chlorosome. Therefore, we believe that the effective refractive index within the pigment aggregate has a value similar to 1.4. The pigment molecules themselves should contribute to the increase in the refractive index inside the chlorosome from the vacuum value.

To evaluate the extent of intensity borrowing, we estimated the ratio of the spectral area of the Q_y band ($area_{Q_y}$) to that of the Soret band ($area_{Soret}$) for both the monomeric BChls *e* and *c* and their chlorosomal aggregates. For the experimental data, the ratio $area_{Q_y}/area_{Soret}$ increased from 0.11 for the monomeric BChl *e* to 0.28 for the *Chl. phaeobacteroides* chlorosome, while it decreased from 0.32 for the monomeric BChl *c* to 0.31 for the *Chl. tepidum* chlorosome. The spectral areas of the Soret band were calculated by integrating the spectra from 17600 to 23800 cm^{-1} and from 20100 to 24600 cm^{-1} for the chlorosomes of *Chl. phaeobacteroides* and *Chl. tepidum*, respectively. Because the estimated spectral areas of the Soret bands for the chlorosomes involved the contribution from the carotenoids, the values of $area_{Q_y}/area_{Soret}$ should be underestimated. The ratio $area_{Q_y}/area_{Soret}$ of the simulated spectra increased from 0.10 for the monomeric BChl *e* to 0.34 for the BChl *e* rodlike aggregate and from 0.29 for the monomeric BChl *c* to 0.42 for the aggregated BChl *c*. Given the underestimation of the experimental values of $area_{Q_y}/area_{Soret}$, the estimated values for the simulated spectra are in good agreement with the experimental results.

To illustrate the extent of the intensity mixings among the B_x, B_y, and Q_y transitions, in Figure 8 we show the contribution from each transition to the isotropic absorption spectra. According to eq 7, $|\boldsymbol{\mu}_m|^2$ can be decomposed into the contributions from the B_x, B_y, and Q_y transitions as

$$|\boldsymbol{\mu}_m|^2 = \boldsymbol{\mu}_m \cdot (\boldsymbol{\mu}_{B_{x,m}} + \boldsymbol{\mu}_{B_{y,m}} + \boldsymbol{\mu}_{Q_{y,m}}) \equiv C_{B_{x,m}} + C_{B_{y,m}} + C_{Q_{y,m}} \quad (10)$$

where $C_{B_{x,m}}$, $C_{B_{y,m}}$, and $C_{Q_{y,m}}$ are the projections of $\boldsymbol{\mu}_m$ to $\boldsymbol{\mu}_{B_{x,m}}$, $\boldsymbol{\mu}_{B_{y,m}}$, and $\boldsymbol{\mu}_{Q_{y,m}}$, respectively. $\boldsymbol{\mu}_{B_{x,m}}$ $\boldsymbol{\mu}_{B_{y,m}}$, and $\boldsymbol{\mu}_{Q_{y,m}}$ are the effective B_x, B_y, and Q_y transition dipoles in the *m*th state, respectively, given in eq 7 and indicate the extent of the mixing of the B_x, B_y, and Q_y transitions in the *m*th state. It should be noted that $C_{Bx,m}$, $C_{B_{y,m}}$, and $C_{Q_{y,m}}$ can be negative. Figure 8 shows the contributions of each transition to the isotropic absorption. The spectra of the B_x (blue), B_y (green), and Q_y (red) contributions in Figure 8 were obtained by substituting $|\boldsymbol{\mu}_m|^2$ in the expressions for the isotropic absorption given by eq 8 with $C_{B_{x,m}}$, $C_{B_{y,m}}$, and $C_{Q_{y,m}}$, respectively. The black lines in Figure 8 show the isotropic absorption spectra, which are the same as those in Figure 7 and correspond to the sum of the other three spectra. Figure 8A clearly shows that in the case of the BChl *e*-containing chlorosome the mixing of the B_y transition accounts for ~40% of the intensity of the Q_y-natured band. On the other hand, the mixing of the B_x transitions with the Q_y-natured band is only minor for the BChl *e*-containing chlorosome and negligible for the BChl *c*-containing chlorosome. This is consistent with the fact that the B_x and Q_y transition dipoles in the neighboring molecules are not in favorable mutual orientations to give strong excitonic couplings.

As discussed by Zimmermann et al. (*28*) in the case of B−Q coupling of the porphyrin aggregate, intensity borrowing works effectively when the difference in the transition-dipole strengths between the two transitions is large. Thus, the larger intensity

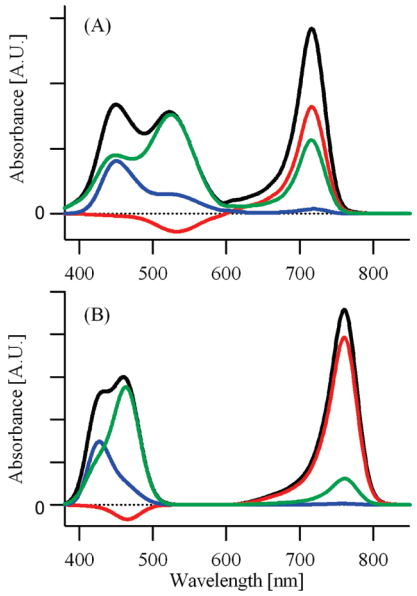

FIGURE 8: Contributions from the B_x (blue), B_y (green), and Q_y (red) transitions to the simulated isotropic absorption spectra (black) for the pigment aggregates composed of BChl *e* (A) and BChl *c* (B). See eq 10 and the related text for details.

borrowing effect for BChl *e* versus that for BChl *c* can be explained by the much larger inequality between the Soret and Q_y transitions in monomeric BChl *e*. The much stronger B_y transition of monomeric BChl *e* versus that of monomeric BChl *c* causes a larger red shift of the B_y-natured band, which results in the stronger coupling between the B_y-natured and Q_y-natured bands and contributes to the further enhancement of the Q_y-natured band, as suggested by Zimmermann et al.

Our simulation suggested that the CD spectra in the Soret region are highly sensitive to a slight alteration in the molecular orientation in the aggregate. This already has been illustrated by Somsen et al. (*44*) and Linnanto and Korppi-Tommola (*27*). In other words, the CD spectra act as a sensitive probe of the structural information of the pigment aggregates, such as chlorosomes. At the same time, the high sensitivity to the structural parameters suggests that there are a number of solutions that could achieve sufficient agreement between the simulated and experimental spectra. In this study, in fact, the adjustments of φ_1 to 60° and of γ_{B_y} and γ_{B_x} to −20° caused an alteration in the LD and CD spectra similar to those caused by the adjustment of φ_1 to 120° and of γ_{B_y} and γ_{B_x} to 20°. Thus, the unambiguous determination of the orientations of the B_x and B_y transition-dipole vectors is outside the scope of this study. Experimental determination of the transition-dipole orientations is necessary to resolve the uncertainty.

Here, we can raise the question of whether the experimental spectra can be well reproduced by structural models that have the same short-range molecular arrangements as the present rodlike model but different higher-order structures. To answer this question, we conducted simulations based on other pigment aggregate models with different higher-order structures versus that of the present rodlike model. We constructed pigment aggregate models with gentler surface curvatures by simply enlarging the radius of the rod with the fixed interstack distance. The number of stacks remained the same, and then the aggregates with the 2- and 4-fold enlarged diameters formed semicylinder and quarter-cylinder structures, respectively. We also constructed a pigment aggregate model with an infinite diameter, which forms

a planar sheet. The short-range pigment arrangements in the stack in the models described above were the same as that in the rodlike model. The simulations based on the semicylinder and quarter-cylinder structures gave basically the same spectral profiles as those simulated on the basis of the rodlike model (data not shown). Thus, our point in this study is that the short-range molecular arrangement assumed in this study, rather than the rodlike higher-order structure, is essential for the accurate reproduction of the experimental spectra. The change from the rodlike to the planar sheet structures had only a limited effect on the simulated absorption spectra. It, however, caused significant changes in the CD spectra. This clearly excludes the possibility of planar sheet being the major structural component of the pigment aggregate.

It has long been known that the CD spectra of the chlorosomes were affected by changes in growth conditions (*45*, *46*), changes in pigment composition (*47*), and the addition and redilution of a saturated hexanol (*48*). These observations indicating the high sensitivity of the CD spectral patterns to various perturbations seem consistent with our simulation also showing the high sensitivity of the CD spectra to the slight changes in the structural parameters. In this simulation, we suggested that the CD spectra in the Q_y region are insensitive to a slight change in the molecular orientation and rather sensitive to the change in the length of the pigment aggregate. It has been known that there is wide variety in the patterns of the CD spectra in the Q_y region among the chlorosomes of different species. The experimental CD spectrum of *Chl. tepidum* showed a small negative band in the red edge region of the Q_y-natured band, while such a negative band was not prominent in the CD spectrum of *Chl. phaeobacteroides*. These observations might suggest the wide variety of the length of the pigment aggregates among species. Saga and Tamiaki (*49*) showed that the CD spectrum of the chlorosome of *Chlorobium vibrioforme* had the opposite sign in the Q_y region versus those of *Chl. phaeobacteroides*. The mechanism inducing such a completely different pattern in the CD spectra of the *Chl. vibrioforme* chlorosome seems unaccountable based on the change in the length of the pigment aggregates, and outside the scope of this study. It is an important issue to be investigated in the future.

It is noteworthy here that Chl *b*, which is abundant in plants, has a molar extinction coefficient similar to that of BChl *e*. Thus, it is likely that the absorption spectrum of Chl *b* is also significantly affected by the intensity borrowing effect when it is included in a densely packed pigment−protein complex, such as light-harvesting chlorophyll−protein complexes (LHCs). Indeed, early work by Oksanen et al. (*50*) and Frąckowiak et al. (*51*) showed that Chl *b* exhibited a similar enhancement of the Q_y band upon self-aggregation. The absorption spectrum of the water-soluble chlorophyll-binding protein reconstituted with Chl *b* alone reported by Theiss et al. (*52*) showed a slightly enhanced Q_y transition. B−Q coupling in LHCs has not been fully discussed and could be an important issue in the future.

CONCLUSIONS

This study indicated the importance of B−Q coupling in the pigment aggregates of chlorosomes, especially those containing BChl *e*. The simulation considering B−B, B−Q, and Q−Q excitonic couplings accurately reproduced the peak positions, relative peak intensities, polarization dependences of the observed absorption spectra, and CD spectra of isolated chlorosomes. The molecular arrangement assumed in the rodlike model was found to be quite suitable for the reproduction of the properties noted above. This study also indicated that the local structure, rather than the higher-order structure assumed in the rodlike model, was essential for the reproduction of the experimental results. In this study, we neglected the effects of the electronic transitions of carotenoids. Because the absorption bands of the carotenoids overlap the B_y-natured band of the BChl aggregates, the contribution of carotenoids should be elucidated in the future. We also neglected the Q_x band and vibronic bands of the Q_y band, which should contribute to the observed low-intensity absorbance between the Soret and Q_y-natured bands. This study indicated the importance of intensity borrowing in BChl *e* and Chl *b* self-aggregates. Quantitative evaluations of intensity borrowing in LHCs will be an important issue in the future.

SUPPORTING INFORMATION AVAILABLE

Definition of the molecular orientation by using the rotating angles, φ_1, θ, and φ_2, shown schematically and molecular arrangements and orientations of the transition dipoles in the structural models used in this study. This material is available free of charge via the Internet at http://pubs.acs.org.

REFERENCES

1. Blankenship, R. E., Olson, J. M., and Miller, M. (1995) Antenna complexes from green photosynthetic bacteria. In Anoxygenic Photosynthetic Bacteria (Blankenship, R. E., Madigan, M. T., and Bauer, C. E., Eds.) pp 399−435, Kluwer Academic Publishers, Dordrecht, The Netherlands.
2. Balaban, T. S., Tamiaki, H., and Holzwarth, A. R. (2005) Chlorins programmed for self-assembly. *Top. Curr. Chem. 258*, 1–38.
3. Montaño, G. A., Bowen, B. P., LaBelle, J. T., Woodbury, N. W., Pizziconi, V. B., and Blankenship, R. E. (2003) Characterization of *Chlorobium tepidum* chlorosomes: A calculation of bacteriochlorophyll *c* per chlorosome and oligomer modeling. *Biophys. J. 85*, 2560–2565.
4. Saga, Y., Shibata, Y., Itoh, S., and Tamiaki, H. (2007) Direct counting of submicrometer-sized photosynthetic apparatus dispersed in medium at cryogenic temperature by confocal laser fluorescence microscopy: Estimation of the number of bacteriochlorophyll *c* in single light-harvesting antenna complexes chlorosomes of green photosynthetic bacteria. *J. Phys. Chem. B 111*, 12605–12609.
5. Griebenow, K., and Holzwarth, A. R. (1989) Pigment organization and energy-transfer in green bacteria. 1. Isolation of native chlorosomes free of bound bacteriochlorophyll-*a* from *Chloroflexus aurantiacus* by gel-electrophoretic filtration. *Biochim. Biophys. Acta 973*, 235–240.
6. Frigaard, N. U., Li, H., Milks, K. J., and Bryant, D. A. (2004) Nine mutants of *Chlorobium tepidum* each unable to synthesize a different chlorosome protein still assemble functional chlorosomes. *J. Bacteriol. 186*, 646–653.
7. Li, H., and Bryant, D. A. (2009) Envelope Proteins of the CsmB/CsmF and CsmC/CsmD Motif Families Influence the Size, Shape, and Composition of Chlorosomes in *Chlorobaculum tepidum*. *J. Bacteriol. 191*, 7109–7120.
8. Gouterman, M. (1978) Optical Spectra and Electronic Structure of Porphyrins and Related Rings. In The Porphyrins (Dolphin, D., Ed.) Vol. III, pp 1−165, Academic Press, New York.
9. Cai, Z. L., Crossley, M. J., Reimers, J. R., Kobayashi, R., and Amos, R. D. (2006) Density functional theory for charge transfer: The nature of the N-bands of porphyrins and chlorophylls revealed through CAM-B3LYP, CASPT2, and SAC-CI calculations. *J. Phys. Chem. B 110*, 15624–15632.
10. Fragata, M., Nordén, B., and Kurucsev, T. (1988) Liner dichroism (250−700 nm) of chlorophyll *a* and pheophytin *a* oriented in a lamellar phase of glycerylmonooctanoate/H_2O. Characterization of electronic transitions. *Photochem. Photobiol. 47*, 133–143.
11. Simonetto, R., Crimi, M., Sandonà, D., Croce, R., Cinque, G., Breton, J., and Bassi, R. (1999) Orientation of chlorophyll transition moments in the higher-plant light-harvesting complex CP29. *Biochemistry 38*, 12974–12983.

12. Linke, M., Lauer, A., von Haimberger, T., Zacarias, A., and Heyne, K. (2008) Three-dimensional orientation of the Q_y electronic transition dipole moment within the chlorophyll *a* molecule determined by femtosecond polarization resolved VIS pump-IR probe spectroscopy. *J. Am. Chem. Soc. 130*, 14904–14905.
13. Linke, M., Theisen, M., von Haimberger, T., Madjet, M. E., Zacarias, A., Fidder, H., and Heyne, K. (2010) Determining the three-dimensional electronic transition dipole moment orientation: Influence of an isomeric mixture. *ChemPhysChem 11*, 1283–1288.
14. Holzwarth, A. R., and Schaffner, K. (1994) On the structure of bacteriochlorophyll molecular aggregates in the chlorosomes of green bacteria. A molecular modelling study. *Photosynth. Res. 41*, 225–233.
15. Pšenčík, J., Ma, Y. Z., Arellano, J. B., Hála, J., and Gillbro, T. (2003) Excitation energy transfer dynamics and excited-state structure in chlorosomes of *Chlorobium phaeobacteroides*. *Biophys. J. 84*, 1161–1179.
16. Prokhorenko, V. I., Steensgaard, D. B., and Holzwarth, A. R. (2003) Exciton theory for supramolecular chlorosomal aggregates: 1. Aggregate size dependence of the linear spectra. *Biophys. J. 85*, 3173–3186.
17. Egawa, A., Fujiwara, T., Mizoguchi, T., Kakitani, Y., Koyama, Y., and Akutsu, H. (2007) Structure of the light-harvesting bacteriochlorophyll *c* assembly in chlorosomes from *Chlorobium limicola* determined by solid-state NMR. *Proc. Natl. Acad. Sci. U.S.A. 104*, 790–795.
18. Staehelin, L. A., Golecki, J. R., Fuller, R. C., and Drews, G. (1978) Visualization of supramolecular architecture of chlorosomes (*Chlorobium*-type vesicles) in freeze-fractured cells of *Chloroflexus aurantiacus*. *Arch. Microbiol. 119*, 269–277.
19. Staehelin, L. A., Golecki, J. R., and Drews, G. (1980) Supramolecular organization of chlorosomes (chlorobium vesicles) and of their membrane attachment sites in *Chlorobium limicola*. *Biochim. Biophys. Acta 589*, 30–45.
20. Saga, Y., and Tamiaki, H. (2006) Transmission Electron Microscopic Study on Supramolecular Nanostructures of Bacteriochlorophyll Self-Aggregates in Chlorosomes of Green Photosynthetic Bacteria. *J. Biosci. Bioeng. 102*, 118–123.
21. Pšenčík, J., Ikonen, T. P., Laurinmäki, P., Merckel, M. C., Butcher, S. J., Serimaa, R. E., and Tuma, R. (2004) Lamellar organization of pigments in chlorosomes, the light harvesting complexes of green photosynthetic bacteria. *Biophys. J. 87*, 1165–1172.
22. Pšenčík, J., Arellano, J. B., Ikonen, T. P., Borrego, C. M., Laurinmäki, P. A., Butcher, S. J., Serimaa, R. E., and Tuma, R. (2006) Internal structure of chlorosomes from brown-colored *Chlorobium* species and the role of carotenoids in their assembly. *Biophys. J. 91*, 1433–1440.
23. Pšenčík, J., Torkkeli, M., Zupčanová, A., Vácha, F., Serimaa, R. E., and Tuma, R. (2010) The lamellar spacing in self-assembling bacteriochlorophyll aggregates is proportional to the length of the esterifying alcohol. *Photosynth. Res. 104*, 211–219.
24. Oostergetel, G. T., Reus, M., Gomez Maqueo Chew, A., Bryant, D. A., Boekema, E. J., and Holzwarth, A. R. (2007) Long-range organization of bacteriochlorophyll in chlorosomes of *Chlorobium tepidum* investigated by cryo-electron microscopy. *FEBS Lett. 581*, 5435–5439.
25. Ganapathy, A., Oostergetel, G. T., Wawrzyniak, P. K., Reus, M., Maqueo Chew, A. G., Buda, F., Boekema, E. J., Bryant, D. A., Holzwarth, A. R., and de Groot, H. J. M. (2009) Alternating *syn-anti* bacteriochlorophylls form concentric helical nanotubes in chlorosomes. *Proc. Natl. Acad. Sci. U.S.A. 106*, 8525–8530.
26. Prokhorenko, V. I., Steensgaard, D. B., and Holzwarth, A. R. (2000) Exciton Dynamics in the Chlorosomal Antennae of the Green Bacteria *Chloroflexus aurantiacus* and *Chlorobium tepidum*. *Biophys. J. 79*, 2105–2120.
27. Linnanto, J. M., and Korppi-Tommola, J. E. I. (2008) Investigation on chlorosomal antenna geometries: Tube, lamella and spiral-type self-aggregates. *Photosynth. Res. 96*, 227–245.
28. Zimmermann, J., Siggel, U., Fuhrhop, J. H., and Röder, B. (2003) Excitonic coupling between B and Q transitions in a porphyrin aggregate. *J. Phys. Chem. B 107*, 6019–6021.
29. Yildirim, H., Işeri, E. I., and Gülen, D. (2004) A quantitative analysis of excitonic superhyperchromism in porphyrin J-/H-aggregates. *Chem. Phys. Lett. 391*, 302–307.
30. Gulen, D. (2006) Significance of the excitonic intensity borrowing in the J-/H-aggregates of bacteriochlorophylls/chlorophylls. *Photosynth. Res. 87*, 205–214.
31. Georgakopoulou, S., van der Zwan, G., Olsen, J. D., Hunter, C. N., Niederman, R. A., and van Grondelle, R. (2006) Investigation of the effects of different carotenoids on the absorption and CD signals of light harvesting 1 complexes. *J. Phys. Chem. B 110*, 3354–3361.
32. Georgakopoulou, S., van der Zwan, G., Bassi, R., van Grondelle, R., van Amerongen, H., and Croce, R. (2007) Understanding the changes in the circular dichroism of light harvesting complex II upon varying its pigment composition and organization. *Biochemistry 46*, 4745–4754.
33. Mizoguchi, T., Kim, T. Y., Sawamura, S., and Tamiaki, H. (2008) Pressure-induced red shift and broadening of the Q_y absorption of main light-harvesting antennae chlorosomes from green photosynthetic bacteria and their dependency upon alkyl substituents of the composite bacteriochlorophylls. *J. Phys. Chem. B 112*, 16759–16765.
34. Harada, J., Miyago, S., Mizoguchi, T., Azai, C., Inoue, K., Tamiaki, H., and Oh-oka, H. (2008) Accumulation of chlorophyllous pigments esterified with the geranylgeranyl group and photosynthetic competence in the *CT2256*-deleted mutant of the green sulfur bacterium *Chlorobium tepidum*. *Photochem. Photobiol. Sci. 7*, 1179–1187.
35. Matsuura, K., Hirota, M., Shimada, K., and Mimuro, M. (1993) Spectral forms and orientation of bacteriochlorophyll *c* and *a* in chlorosomes of the green photosynthetic bacterium *Chloroflexus aurantiacus*. *Photochem. Photobiol. 57*, 92–97.
36. Tamiaki, H., Tateishi, S., Nakabayashi, S., Shibata, Y., and Itoh, S. (2010) Linearly polarized light absorption spectra of chlorosomes, light-harvesting antennas of photosynthetic green sulfur bacteria. *Chem. Phys. Lett. 484*, 333–337.
37. Knox, R. S. (2003) Dipole and oscillator strengths of chromophores in solution. *Photochem. Photobiol. 77*, 492–496.
38. Gurzadyan, G. G., Tran-Thi, T. H., and Gustavsson, T. (1998) Time-resolved fluorescence spectroscopy of high-lying electronic states of Zn-tetraphenylporphyrin. *J. Chem. Phys. 108*, 385–388.
39. Mataga, N., Shibata, Y., Chosrowjan, H., Yoshida, N., and Osuka, A. (2000) Internal conversion and vibronic relaxation from higher excited electronic state of porphyrins: Femtosecond fluorescence dynamics studies. *J. Phys. Chem. B 104*, 4001–4004.
40. Liu, X., Yeow, E. K. L., Velate, S., and Steer, R. P. (2006) Photophysics and spectroscopy of the higher electronic states of zinc metalloporphyrins: A theoretical and experimental study. *Phys. Chem. Chem. Phys. 8*, 1298–1309.
41. Borrego, C. M., Arellano, J. B., Abella, C. A., Gillbro, T., and Garcia-Gil, J. (1999) The molar extinction coefficient of bacteriochlorophyll *e* and the pigment stoichiometry in *Chlorobium phaeobacteroides*. *Photosynth. Res. 60*, 257–264.
42. Oelze, J. (1985) Analysis of bacteriochlorophylls. *Methods Microbiol. 18*, 257–284.
43. Kleima, F. J., Hofmann, E., Gobets, B., van Stokkum, I. H. M., van Grondelle, R., Diederichs, K., and van Amerongen, H. (2000) Förster excitation energy transfer in peridinin-chlorophyll-*a*-protein. *Biophys. J. 78*, 344–353.
44. Somsen, O. J. G., van Grondelle, R., and van Amerongen, H. (1996) Spectral broadening of interacting pigments: Polarized absorption by photosynthetic proteins. *Biophys. J. 71*, 1934–1951.
45. Lehmann, R. P., Brunisholz, R. A., and Zuber, H. (1994) Structural differences in chlorosomes from *Chloroflexus aurantiacus* grown under different conditions support the BChl *c*-binding function of the 5.7 kDa polypeptide. *FEBS Lett. 342*, 319–324.
46. Arellano, J. B., Pšenčík, J., Borrego, C. M., Ma, Y. Z., Guyoneaud, R., Garcia-Gil, J., and Gillbro, T. (2000) Effect of carotenoid biosynthesis inhibition on the chlorosome organization in *Chlorobium phaeobacteroides* strain CL1401. *Photochem. Photobiol. 71*, 715–723.
47. Steensgaard, D. B., van Walree, C. A., Permentier, H., Bañeras, L., Borrego, C. M., Garcia-Gil, J., Aartsma, T. J., Amesz, J., and Holzwarth, A. R. (2000) Fast energy transfer between BChl *d* and BChl *c* in chlorosomes of the green sulfur bacterium *Chlorobium limicola*. *Biochim. Biophys. Acta 1457*, 71–80.
48. Wang, Z. Y., Marx, G., Umetsu, M., Kobayashi, M., Mimuro, M., and Nozawa, T. (1995) Morphology and spectroscopy of chlorosomes from *Chlorobium tepidum* by alcohol treatments. *Biochim. Biophys. Acta 1232*, 187–196.
49. Saga, Y., and Tamiaki, H. (2004) Comparison between chlorosomes containing bacteriochlorophyll-*c* and chlorosomes containing bacteriochlorophyll-*d* isolated from two substrains of green sulfur photosynthetic bacterium *Chlorobium vibrioforme* NCIB 8327. *J. Photochem. Photobiol., B 75*, 89–97.
50. Oksanen, J. A. I., Helenius, V. M., Hynninen, P. H., van Amerongen, H., Korppi-Tommola, J. E. I., and van Grondelle, R. (1996) Circular and linear dichroism of aggregates of chlorophyll *a* and chlorophyll

b in 3-methylpentane and paraffin oil. *Photochem. Photobiol. 64*, 256–362.
51. Frąckowiak, D., Goc, J., Malak, H., Planner, A., Ptak, A., and Zelent, B. (1996) Aggregation of chlorophyll b in model systems. *J. Photochem. Photobiol., A 94*, 43–51.
52. Theiss, C., Trostmann, I., Andree, S., Schmitt, F. J., Renger, T., Eichler, H. J., Paulsen, H., and Renger, G. (2007) Pigment-pigment and pigment-protein interactions in recombinant water-soluble chlorophyll proteins (WSCP) from cauliflower. *J. Phys. Chem. B 111*, 13325–13335.